Quantum devices

Internship report

Biosensors for detection of bacteria using fluorescence

Author: Elisa Passalacqua

Tutors: Dr Anne Chantal Gouget
Cassiana Andrei, PhD student
Professor Carlo Ricciardi

Location: Laboratoire de Physique de la Matière Condensée,
École Polytechnique, IPP

March-June 2019

Contents

1 Introduction

Nowadays there is an increase demand for diagnostic devices that can allow a fast and accurate detection of pathogenic bacteria for a variety of different applications, from food control to early medical diagnosis. Conventional bacteria diagnostic utilized still relies on classical microbiology methods, which require several steps, trained personnel and can take days. As a response to these disadvantages several techniques are currently being investigated, among which there are the optical biosensors. In general a biosensor is described as a device capable of converting a biological response into a readable signal, thanks to the presence of biological detecting elements and a sensor element that transduces the signal[1]. These devices present several advantages, among which the fact that they are less time consuming than conventional methods (the timescale can be of less than an hour), they can have an higher sensitivity (which can contribute to the decrease of the response time), they can be highly specific and they can be miniaturized (decreasing also the costs).
In the laboratory PMC previous studies were conducted on fluorescence biosensors, based, in particular, on a robust and reproducible surface chemistry for the grafting of probes on an amorphous silicon-carbon alloy surface through strong Si-C covalent bonds and on the enhancement of the optical signal due to the presence of a nanostructured metallic layer (metal-enhanced fluorescence), which allowed, for example, the implementation of a highly sensitive and specific biochips, which, compared to biosensors, offer multiplex detection simultaneusly[2−3].
Following these studies, the main objective of this internship has been to verify the feasibility of using the developed architecture for the optical detection of bacteria, in this case *Escherichia Coli*, via mannoside probes. In fact, mannoses can have specific interactions with *E. Coli* bacteria due to the presence of the type I FimH fimbriae on the *E. Coli* as the distal end adhesin protein, which are composed of two domains, a receptor-binding lectin domain that functions as a mannose-specific adhesin for recognition and binding to the host cell and a pilin domain allowing copolymerization that exposes an hydrophobic core [4−5]. Thus, α-propargyl mannosides are grafted onto the bio-sensor surface as the capture-agents used to immobilize the bacteria (*Escherichia Coli*) while the optical signal is generated by a second labelled mannose (mannopyranoside derivates conjugated to Cyanine 5), deposited afterwards in a sandwich architecture (composed by a mannose-bacteria-mannose interaction and shown in Fig 1), and used to recognize the presence of the target and, due to its fluorescence properties that are amplified by the presence of the nanostructured metallic layer, is the 'sensor' element that transduce the interaction with the bacteria into a readable signal.

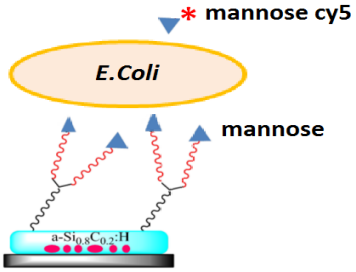

Figure 1: Scheme of the sensor with sandwich architecture

As mentioned above, the signal obtained from the bio-sensor is an optical one, due to the presence of a fluorophore, an element capable of spontaneously emitting light once it is brought to an excited state (usually by a photon absorption), which is enhanced by the coupling with the plasmons of the underlying metal layer. In fact, the presence of the latter alters the 'free space' conditions of the molecular dipole radiation, acting as an optical antenna and increasing the excitation rate of the fluorophores, thanks to the local field enhancement obtained by the interaction between the light and the metal surface, and modifying its radiative and non-radiative decay rates[6]. Thus, several factors have to be taken into consideration when designing this kind of sensors. In particular, one has to properly choose the metallic substrate (in terms of material, morphology and size, since they can vary the optical resonant conditions) and fluorophore utilized in order to provide an overlap of the optical properties, taking into consideration also the wavelength of the excitation field. Moreover, the distance between the metallic layer and the fluorophore has to be optimized as well, to avoid quenching effects due to the increase of the non-radiative rate at close proximity, and a spacer material may be needed to tune it.
Moreover, the enhancement of the local field leads also to an enhancement of the Raman scattering (the inelastic scattering of a photon by molecules which are excited to higher energy levels), in what is called the surface-enhanced Raman scattering, which could be exploited as a further readable signal of the biosensor that allows also the identification of the immobilized bacteria, due to presence of characteristic peaks in the Raman shift, or simply to verify the presence of the local field enhancement due to the metallic layer.

2 Experimental section

2.1 Materials

All chemicals were used as received, without further purification. Ultrapure water (Milli-Q, 18 MΩ cm^{-1}) was used as buffer and for the rinsing steps. All cleaning (H_2O_2 30%, H_2SO_4 96%, Acetic acid glacial) and etching (HF 50%) reagents were of RSE grade and purchased from Carlo Erba. Undecylenic acid 99% was supplied by Acros organics, Rhodamine B by Fluka, 10X PBS (phosphate buffer saline) buffer pH 7.4 by Ambion, MeO-PEG-alkyne (PEG750 / PEG2000) by Iris Biotech, Lectin PNA Alexa Fluor 647 conjugated by Life technologies and Alexa Fluor 647 NHS-ester by Eurogentec. Alexa Fluor 647 labelled Concavaline A (ConA), Lectin PNA (from Arachis hypogaea) and Alexa Fluor 594 labelled Lectin PNA (from Arachis hypogaea) were purchased from Molecular probes Invitrogen. Propargyl α-D-mannopyranoside and propargyl β-D-lactoside were supplied by Synthose. The fluorescence antibodies and the Mannopyranoside derivates conjugated to Cyanine 5 were given by the laboratory IRI at Villeneuve d'Ascq, while the 2x TY and LB media and the Chloramphenical, Kanamycine, Ampicillin antibiotics were given by the Biochemistry laboratory at the École Polytechnique. Ethylenedinitrilo tetraacedic acid, disodium salt dihydrate (EDTA) and Phosphate were purchased from Merck while Tween 20 was purchased by Calbiochem. All the other chemicals of the highest available quality were purchased from Sigma-Aldrich.

2.2 Slides preparation

The bare glass slides used as a substrate were prepared starting from microscope glass slides that were thoroughly cleaned with deionized water and TFD4 detergent (Franklab), put in ethanol and mixed for 15 minutes, carefully rinsed with deionized water and Milli-Q, immersed in a piranha solution (1/3 H_2O_2/H_2SO_4, which is very corrosive and has to be handled carefully), cleaned again in Milli-Q and finally dried. The different slides with a nano-structured metallic layer (4 nm Au, 4 nm Ag or 4 nm Au with an adhesive layer of 4 nm Ti) used were provided from Lille.
The annealing was performed using a rapid thermal annealer (Jipelec Jet First 100) at 500° for 1 minute under argon atmosphere.
The amorphous silicon-carbon alloy ($aSi_{1-x}C_x$:H) was deposited using plasma-enhanced chemical vapour deposition (PECVD) from SiH_4 and CH_4 precursors at a controlled substrate temperature (150°C-250°C) and pressure (40 mTorr in the chamber) in a

capacitively coupled reactor used in low power regime (power density 0.1 W/cm^2, RF signal at 13.6 MHz). The carbon composition was tuned by changing the CH_4 precursor ratio with respect to the total gas in the chamber while the thickness of the final deposited layer was fixed by the deposition time.

2.3 Surface functionalization for the fabrication of the sensor

To implement the sensor architecture several steps were required. Starting from the amorphous silicon-carbon alloy layer ($aSi_{1-x}C_x$), the surface was at first etched in HF vapour for 15 s and subsequently immersed in a degassed schlenk tube, where the undecylenic acid had been heated and flushed with Ar beforehand at 100°C and left to cool down, for 15 minutes before being inserted in a UV chamber where it was irradiated at 312 nm and 6 mW/cm^2 for 3 hours. The reacted surface was then rinsed for three times with acetic acid at 75°C for 20 minutes and dried under a nitrogen flow.
The slide was then inserted into a schlenk tube containing an aqueous solution of N-Hydroxysuccinimide (NHS) 10 mM and of N-(3-dimethylaminopropyl) - N'-ethylcarbodiimide hydrochloride (EDC) 10 mM in equal volume and flushed with Ar at 15°C for 1.30 h. After a rigorous rinsing in Milli-Q and a drying under a nitrogen flow, the slide was put in a schlenk tube with L-glutamic acid 20 mM and pH 8 for 3 hours at room temperature, following which the slide was cleaned in four steps (in PBS 1X SDS 0.1% for 15 minutes, in PBS 0.2X for 2 minutes, in PBS 0.1X for 2 minutes and in Milli-Q for 2 minutes) and dried under a nitrogen flow.
For a second time the slide was placed into a schlenk tube containing the aqueous solution of NHS 10 mM and of EDC 10 mM and flushed with Ar at 15°C for 1.5 h. For the samples containing a metallic layer, this was followed by a further immersion of the slide in a schlenk tube containing o-(2-aminoethyl) -o'- (2-azidoethyl)nonaethyleneglycol ($NH_2EG_{10}N_3$) 20 mM in PBS 1X with pH 8 for 3 hours at room temperature and by four cleaning steps (in PBS 1X SDS 0.1% for 15 minutes, in PBS 0.2X for 1 minutes, in PBS 0.1X for 1 minutes and in Milli-Q for 99 s) and a drying step under a nitrogen flow.
Several lines of propargyl glycans and of a fluorescent dyes were spotted onto the slide by a spotter robot, used in a controlled environment (temperature ∼15°C and humidity ∼ 50%). In particular, propargyl alcool 3 mM in PTS buffer (10 mL Phosphate 0.3 M, 50 μL Tween 20 at 1%, 20 μL Sarkosyl 0.5%) with sodium L-ascorbate 0.45 mM and copper (II) sulfate pentahydrate ($CuSO_4$) 0.15 mM, propargyl mannoside 3 mM in PTS buffer with sodium L-ascorbate 0.45 mM and $CuSO_4$ 0.15

mM, propargyl lactoside 3 mM in PTS buffer with sodium L-ascorbate 0.45 mM and $CuSO_4$ 0.15 mM and propargyl Alexa Fluor 647 0.1 mM in PTS buffer with sodium L-ascorbate 150 μM and $CuSO_4$ 5 μM were used for the different lines. After spotting the slide was left in a desiccator with a controlled humidity overnight.
Lastly, MeO-PEG-alkyne (PEG750 Alkyne or PEG2000 Alkyne) 3 mM (20 mM) in PTS buffer with sodium ascorbate 0.6 mM (4 mM) and $CuSO_4$ 0.17 mM (1.13 mM) was deposited on the slide for 2 hours, which was then rinsed in EDTA 0.1 M, cleaned in PBS 1x SDS 0.1% for 15 minutes, in PBS 0.2x for 1 minute, in PBS 0.1x for 1 minute and in Milli-Q for 99 s and was dried under a nitrogen flow.
For the last sample used, composed by the glass slide on top of which the amorphous Si layer was deposited, after the slide was was placed into a schlenk tube containing the aqueous solution of NHS 10 mM and of EDC 10 mM and flushed with Ar at 15°C for 1.5h for the second time, after which it was once again immersed in a shlenck tube containing Carboxy-PEG_{12}-Amine 10 mM in PBS 1X with pH 8 for 3 hours at room temperature and cleaned in four steps (inPBS 1X SDS 0.1% for 15 minutes, in PBS 0.2X for 1 minutes, in PBS 0.1X for 1 minute and in Milli-Q for 99 s) and a drying step under a nitrogen flow. A third activation of the sample in a schlenk tube containing the aqueous solution of NHS 10 mM and of EDC 10 mM and flushed with Ar at 15°C was repeated for 1.5h. This was followed by the spotting (using the spotter robot) of the aminophenylmannopiranoside 8 mM in a KH_2PO_4 pH 9 buffer. After the spotting, the slide was left in the spotter with a controlled humidity and temperature overnight.

2.4 Bacteria growth conditions

The growth of all the bacteria strain was performed in the Biochemistry laboratory at the École Polytechnique. The *E. Coli* Katushka strain (obtained from the *E.Coli* K12 MG1655 (ATCC 700926) with the pDONR221-nadB-cat recombinant plasmid[8]) was grown in 20 mL of 2x TY media with 20 μL of chloramphenicol / isopropanol 34 mg/mL and 20 μL of kanamycin 25 mg/mL and left overnight in a rotating oven (at 37°C and 200 rps), after which the bacteria was extracted from the media through centrifugation and put in PBS 1x, from which the optical density at 600 nm was measured to calculate the concentration of the bacteria (considering that an optical density value of 0.644 at 600 nm corresponds to 10^{11} cfu/mL).
The *E. Coli* pUT pMM strain (obtained from plasmid-transform AAEC185[9]) was grown in 5 mL of Lysogeny broth (LB) media with 3.67 μL of chloramphenicol / isopropanol 34 mg/mL and 40 μL Ampicillin 12.5 mg/mL and left overnight in a rotating oven (at 37°C and 200 rps). Afterwards, 200 μL of the night culture were added to 20 mL of LB and 20 μL of isopropyl-ß-D-thiogalactopyranoside (IPTG) 1

M and the solution was left in an oven at 37°C for 48 hours. Lastly, the bacteria was extracted from the media through centrifugation and put in PBS 1x, from which the optical density at 600 nm was measured to calculate the concentration of the bacteria (considering that an optical density value of 0.644 at 600 nm corresponds to 10^{11} cfu/mL).

2.5 Bacteria deposition and sandwich architecture

Both the bacteria grown (Katushka and pUT pMM) were diluted in PBS 1X from the concentration found by the optical desnity measurement to 10^8 cfu/mL and deposited on the surface for 1 h, followed by a rinsing in PBS 1X for 5 minutes and in Milli-Q for 2 minutes. The Mannopyranoside derivates conjugated to Cyanine 5 were deposited, in different molar concentrations in PBS Tween 0.005%, for 15 minutes on the sample and rinsed in PBS 1X (in later experiments in PBS Tween 0.005%) for 5 minutes and in Milli-Q for 2 minutes (in later experiments a second rinse in PBS SDS 0.1% for 5 minutes and in Milli-Q for 2 minutes was added)

2.6 Characterization and measurements

UV-visible spectrometer
The absorption spectra of the slides were obtained with a Cary 300 spectrometer in the range 200-800 nm.

Raman measurements
The Raman spectra were obtained with a confocal Raman microscope (CRM alpha 300R) using the 633 nm He-Ne laser to excite the samples with an acquisition time of 30 s, a laser power of typically 2.5 mW (obtained with a 10% filter but tunable in order to avoid saturation or photo-degradation of the samples), a collection hole diameter of 100 μm and were measured in the 200-2200 cm^{-1} range.

Fluorescence measurements
The fluorescence measurements were obtained with an Innoscan 710, which allowed the use of a laser at 532 nm (Cy3) and one at 635 nm (Cy5). The lasers were used in low laser power regime (5 mW) and the gain was tuned during the experiments (it is referred hereafter as a percentage of the total laser power).

Spotter
The spotting process is carried out by a spotter robot (Biorobotics MicroGrid II), where the slides are immobilized in programmed positions while a spotting needle deposits by contact the spotting solutions (20 μL of each solutions are placed in a microplate according to the programmed sequence). The spotting process takes place under controlled humidity ($\sim$ 50%) and temperature ($\sim$ 20°C). The spotted samples are stored in a desiccator (with a controlled humidity of $\sim$ 75%) overnight.

3 Experimental results

3.1 Study of the optical properties of nanostructured noble metal substrates

The two most commonly used materials in plasmonic applications, when working at wavelengths in the visible or near-infrared, are gold and silver, due to their optical properties, availability and ease of manipulation[7].

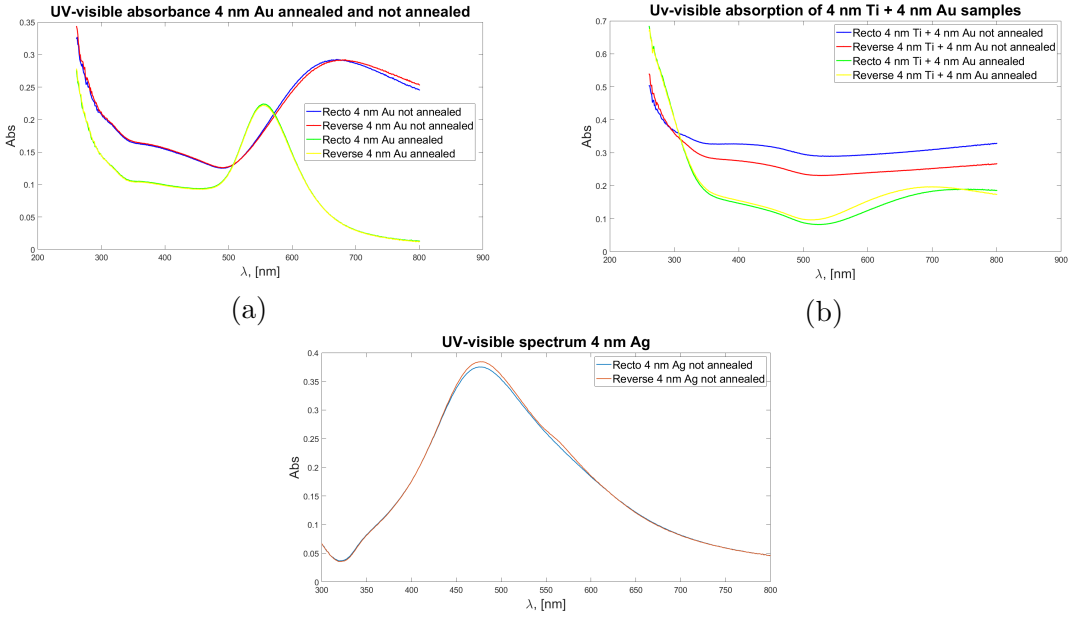

Figure 2: UV-visible absorption spectra for the 4 nm Au samples (a), 4 nm Ti and 4 nm Au samples (b) , not annealed (red and blue lines, taken at the opposite edges of the slide) and annealed (green and yellow lines, taken at the opposite edges of the slide), and 4 nm Ag sample (c)

In this section, five different substrates based on these materials are examined,

starting from the localized surface plasmon resonance response (obtained by the UV-visible absorbance measurement and visible in Fig 2). The substrates were chosen considering previous optimization of the thickness of the layer for the metal-enhanced fluorescence response and consists of two samples where 4 nm of Au were deposited by thermal evaporation starting from a Au thin film, one of which was later thermally annealed, two samples where 4 nm of a Ti adhesion layer, used as protection and to increase the homogeneity of the nano-structured metallic layer, were deposited before the 4 nm of Au, one of which was later thermally annealed, and one sample where 4 nm of Ag were deposited by thermal evaporation starting from a Ag thin film.

For each substrate the UV-visible absorbance was measured in two opposite points on the surface (called recto and reverse in Fig 2) in order to study the spatial homogeneity of the substrates. From the UV-visible spectra it is possible to make several remarks. Starting from Fig 2a, which shows the absorbance of the two Au substrates, it is possible to notice that the plasmon resonance shifts after the annealing process from $\sim$ 677 nm (672 nm in the recto measurement and 683 nm in the reverse) to $\sim$ 555 nm (555 nm in the recto measurement and 556 nm in the reverse one). Moreover, one can easily observe that the plasmon resonance of the not annealed substrate results broader than the one obtained after the thermal treatment. These considerations can be explained by a decrease of the size of the nanoparticles after the annealing. In fact, usually as the size of the nanoparticles in the metallic layer increases the plasmonic resonance is red-shifted and broadened due to the fact that at larger diameters the scattering tends to dominate with respect to the absorption on the measured extinction of the light, increasing the damping of the resonance and decreasing the quality factor. However, it can be observed that in the annealed Au samples taken into consideration the value of the absorption at resonance tends to be increased when the sample is not annealed (associated with larger NPs). This can be explained by the fact that Au is strongly affected by optical absorption at $\lambda < 600$ nm, due to the presence of inter-band transitions in the material at these frequency, which are less relevant at higher wavelengths[7].
Considering the spectra shown in Fig 2*b*, where an adhesion layer of 4 nm of Ti was added, it is possible to make similar remarks concerning the effect of the thermal treatment on the plasmonic properties of the surface. In fact, even in this case, a blue-shift can be observed due to the annealing process, with the resonance moving from wavelengths higher than 800 nm (thus not visible in the measurements) to $\sim$ 726 nm (756 nm in the recto measurements and 696 nm in the reverse), accompanied by a decrease in the absorbance values. While it is not possible to study directly the effect of the adhesion layer on the Au substrate, it is possible to notice a remarkable broadening of the spectra with respect to the ones obtained by the Au samples previously discussed. This, coupled with a red-shift and a decrease in the magnitude

of the resonance, has been observed several times in literature[10−11] and is thought to be due to the high optical absorption of the adhesion layer, especially when the latter is metallic, which leads to a stronger damping of the plasmonic resonance. Moreover, in this substrate it is possible to notice that the spatial homogeneity of the surface is lower with respect to the one found in the Au samples, even after the annealing process.
Finally, from Fig 2c, where the not annealed Ag sample spectra is shown, it is possible to observe the effect of the material on the UV-visible absorption. In fact, for silver, the plasmonic resonance is usually found at lower wavelength due to the different dielectric constant (in the sample the resonance wavelength value is found at 476 nm in the recto measurement and 477 nm in the reverse one). Moreover, due to the lower absorption (ϵ_∞), the absorbance at resonance of the Ag sample is the higher than the one found with the Au samples.

Having examined the plasmon response for all the different substrates available, the second step is to verify the effect of the metallic layer on the SERS and fluorescence response of the sample. This was done by depositing on the surface droplets of two well-known dyes, rhodamine B (RhB, which has an absorption wavelenght of $\lambda_{abs} \sim 554$ nm and an emission wavelength at $\lambda_{emi} \sim 583$ nm in solution with water) and crystal violet (CV, which has an absorption wavelenght of $\lambda_{abs} \sim 590$ nm and an emission wavelength at $\lambda_{emi} \sim 635$ nm in solution with water) with different concentrations (10^{-4} M and 10^{-5} M) and comparing the results obtained with the different samples (shown in Fig 3, 4 and 5).

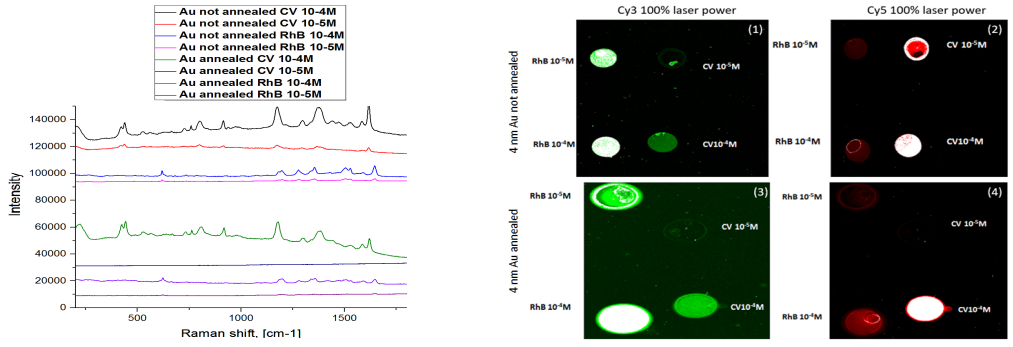

(a) (b)

Figure 3: SERS spectra (a) and fluorescence measurements (b) for the 4 nm Au not annealed sample (top measurements) and the 4 nm Au annealed sample (bottom measurements)

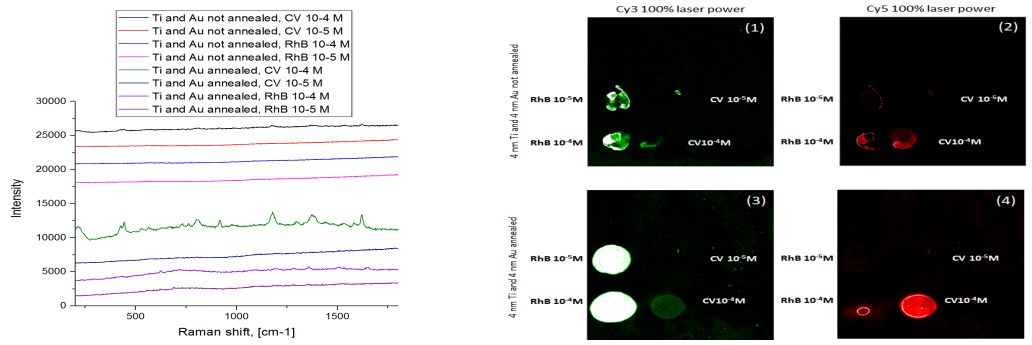

(a) (b)

Figure 4: SERS spectra (a) and fluorescence measurements (b) for the 4 nm Ti and 4 nm Au not annealed sample (top measurements) and the 4 nm Ti and 4 nm Au annealed sample (bottom measurements)

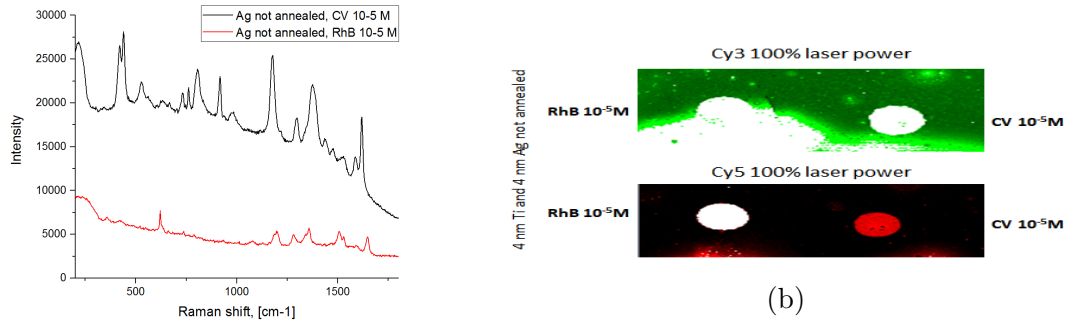

(a) (b)

Figure 5: SERS spectra (a) and fluorescence measurements (b) for the 4 nm Ag not annealed sample

To interpret the results found for every substrate one needs to take into consideration both the aforementioned characteristic wavelengths of the dyes and the ones of the excitation laser (633 nm in the case of the Raman measurements while, for the fluorescence measurements, the cy3 laser is associated with a wavelength of 532 nm while the cy5 laser with 635 nm) and how these are coupled with the plasmon resonance of the metallic layers. In fact, starting from the not annealed Au sample (Fig 3, top measurements), the Raman spectra of both the dyes, even at the lowest concentration, present clear characteristic peaks, with higher intensity measured in the case of the CV (so much so that, while the rest of the measurements where taken with 10% of the laser power, for the case of the CV with a concentration of 10^{-4} M it was decreased to 5% to avoid saturation). This could be explained by the fact that the dye has a wavelength of absorption closer to the laser excitation and to the plasmon resonance of the substrate, with respect to the one of the RhB. Likewise, in fluorescence it is possible to observe a clear response from all the droplets, with a stronger signal coming from the RhB when the laser utilized is cy3 and from CV

using cy5. However, once, due to the thermal annealing, the plasmon resonance is blue-shifted, the Raman and fluorescence signal coming from the CV with the lowest concentration are no longer visible, as shown in Fig 3 (bottom measurements), even when, also in this case, the signal observed from the CV 10^{-4} M was taken using just 5% of the laser power. In general, when comparing the intensity of the SERS signal between the annealed and not annealed Au samples, the former has higher values, which could be explained by the closeness of its plasmon resonance wavelength to the excitation laser.
Considering the samples with the Ti adhesion layer (Fig 4), a degradation of the Raman signal with respect to the previous samples is immediately visible. In fact, in both the not annealed (top measurements) and annealed (bottom measurements) cases, only the CV 10^{-4} M has clear peaks, whereas in the rest of the spectra is not possible to distinguish the signal from the noise. This could be explained by the fact that the plasmonic resonance is shifted towards high wavelength, especially in the not annealed case, where the intensity of the Raman shifts found is lower, or by the damping due to the absorption of the Ti layer (which is linked to the broadening found in the UV-visible spectra). However, the fluorescence signal, albeit weaker in the CV case, is still easily observable. This may be due to the fact that, while the medium losses lead to a decrease in the local field enhancement and have a detrimental effect on both the enhanced-fluorescence and SERS capability of the substrate, the fluorescence decay rate may be primarily effected by the Au layer[12].
Lastly, for the Ag substrate response (shown in Fig 5), only the lowest concentration of the two dyes were deposited, since clear signal were observable in both cases (in the CV case so much so that, to avoid saturation the laser power used was of just 3.2%). This seems to be in contrast with the observations done until now, since, as seen above, the plasmon resonance in this material is at very low wavelengths, quite far from both the laser excitation and the dyes absorption wavelengths. This can be explained by the fact that, as seen in the description of the UV-visible spectra, the low absorption of silver leads to higher values of the absorbance even at wavelengths far from the resonance while maintaining the characteristic peak-shape, allowing for a larger margin of coupling.

Having considered these results, three different kind of substrate were chosen to implement the amorphous architecture: the 4 nm nano-structured Au not annealed and annealed and the 4 nm nano-structured Ag not annealed. On top of these substrates a further spacer layer of amorphous silicon-carbon, used as the base for the chemical functionalization, was deposited by PECVD at low power regime, as described above. The carbon content and thickness of this layer have been previously optimized by the group in terms of optical transparency and of distance between the nanoparticles and the immobilized proteins formerly studied, respectively (3 nm of

$aSi_{80\%}C_{20\%}$ for the Au substrates and 5 nm of $aSi_{95\%}C_{5\%}$ for the Ag one). Moreover, the deposit had to be performed at temperature included between 250°C (for the Au substrates) and 150°C (for the Ag one) in order to incorporate enough H atoms in the aSiC structure ($aSi_{1-X}C_X$:H), necessary to passivate the dangling bonds present in the layer. The deposition of the amorphous layer on top of the metallic one leads to a variation in the plasmon resonance of the samples, observed by the UV-visible absorption characterization (Fig 6), since the electromagnetic properties of the nanoparticles are affected by the environment[7]. In fact, it is possible to notice a red-shift of the resonance due to the increase in the dielectric constant of the substrate. This is less evident in the not annealed gold sample, where the variation to the resonance wavelength is just of $\sim$ 7 nm. This may be due to a partial annealing that may have happened during the PECVD (performed at 250°C) linked to an instability of the nanoparticles, that would have caused a red-shift in the plasmon peak. The final plasmonic resonance obtained in the different substrates were at 603 nm in the case of the not annealed Au substrate, at 573 nm for the annealed Au substrate and at 577 nm in the Ag substrate, values close to the best coupling of the LSPR with the cy5 fluorophore found previously by the group using a similar coating (λ_{LSPR}= 614 nm).

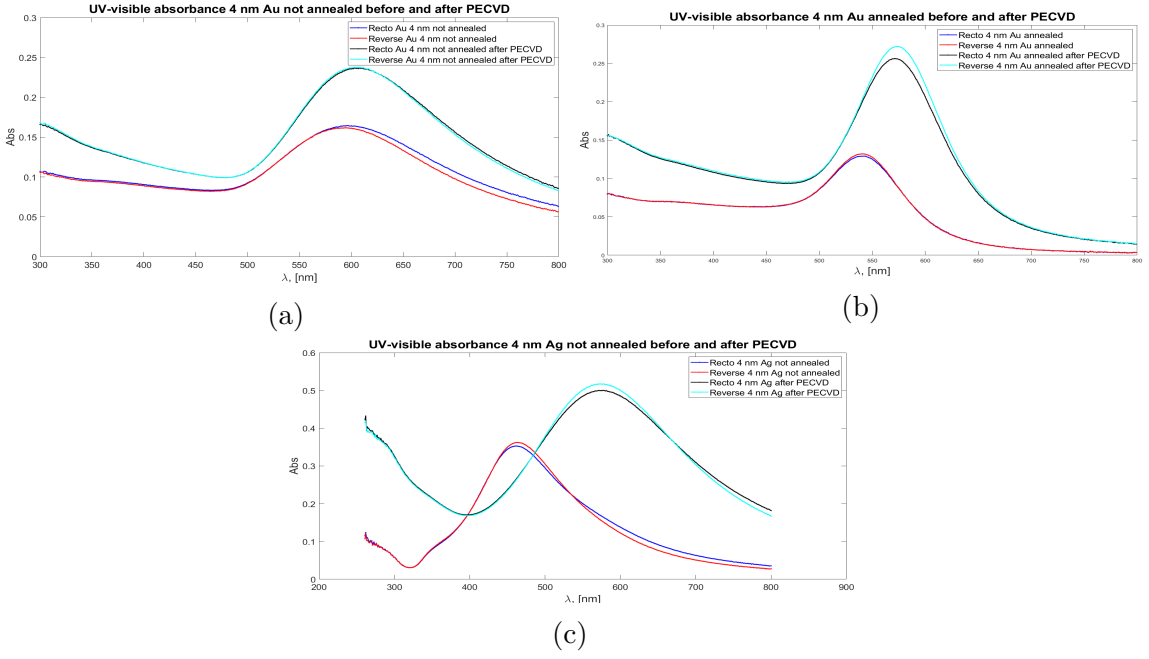

Figure 6: UV-visible absorption spectra for the 4 nm Au not annealed sample (a), 4 nm Au annealed sample (b) and 4 nm Ag sample (c)

3.2 Fabrication of the glycan biochip

The bacteria sensor was developed starting by the aforementioned surface chemistry developed by the group, that leads to the grafting of glycans on the hydrogenated amorphous silicon-carbon alloy ($aSi_{1-x}C_x$:H) surface by click chemistry. This functionalization of the surface for the implementation of the sensor is composed by 5 steps (shown in Fig 7). The first step consists in the formation of Si-H bonds obtained by the etching of the amorphous layer, performed using just the HF vapours. This is followed by a photo-activated hydrosilylation reaction of the undecylenic acid, taking place on the Si-H bonds, and resulting in the formation of a carboxydecyl-terminated monolayer attached to the top of the surface by Si-C bonds. A thorough rinse with hot acetic acid is then needed to eliminate the unreacted undecylenic acid. Afterwards, two successive amidation reactions are performed in a physiological buffer to attach the azido functions. The acid functions present on the surface are first activated by the use of a coupling reagent (EDC) in the presence of NHS to form a quasi stable active NHS-ester termination, then an aminolysis reaction is carried out with the glutamic acid, needed to increase the grafting density of the $aSi_{1-x}C_x$:H layer as a result of the two acid branches. This is followed by a second activation, identical to the previous one, and by a further amidation reaction with an amino oligo(ethylene glycol) ($NH_2EG_{10}N_3$) terminated by an azido function, which provides a first anti-fouling layer to prevent non specific adsorption of unwanted bacteria or proteins present in complex media. In the last step the propargyl-terminated glycans can be bound to the system through the Cu(I)-catalyzed Huisgen 1,3- dipolar cycloaddition (click chemistry) through the use of the spotter. In particular, four types of molecules were used: 1) propargyl mannoside, used as the bio element to interact specifically with the *E. Coli* bacteria (both the Katushka and the pUT pMM strains) and with the protein ConA, 2) propargyl lactoside, used as the bio element to interact specifically with Lectin PNA, 3) propargyl alcohol, used to verify the presence of non specific interactions and 4) propargyl Alexa Fluor 647, used to delimit the zones of the sensor. The layout of the first sample used is shown in Fig 7, where the sample was divided in four identical spotted zones. After the spotting, in a last step, all the unreacted azido functions are blocked using methoxy PEG750-propargyl in order to create a second antifouling layer. The poly(ethylene glycol) (PEG) is a commonly used blocking material, whose antifouling properties are linked to the hydrophilic behaviour of its chain, obtained by the formation of hydration layers due to the hydrogen bonds with water, and to steric hindrance effects present for long-chained PEG, which enables the compounds to act as a physical barrier for the protein and bacteria adsorption[13].

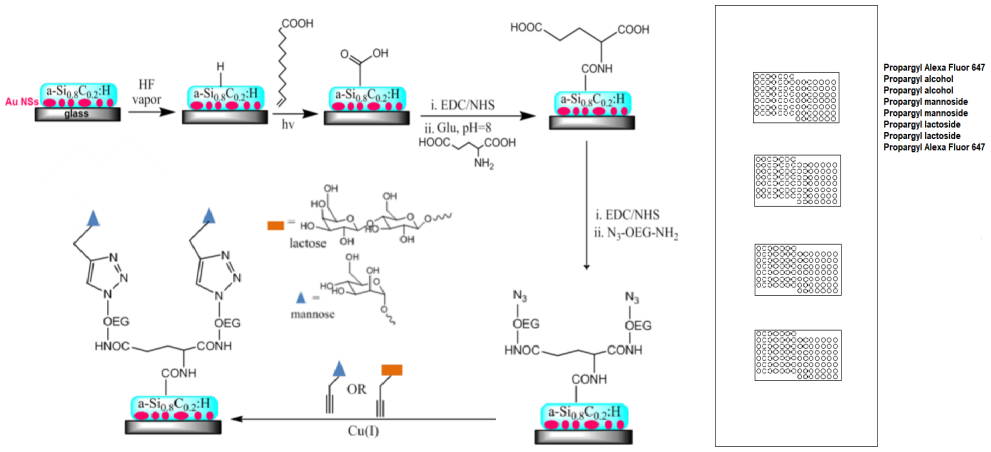

(a) (b)

Figure 7: Functionalization scheme (a) and slide layout (b)

3.3 *E. Coli* Katushka deposition

The first substrate used was the annealed 4 nm Au with the 3 nm $aSi_{80\%}C_{20\%}$:H layer. After the surface functionalization, the Katushka strain of *E. Coli*, in which the expression of the katushka near-infrared fluorescent protein (λ_{abs}= 588 nm, λ_{em}= 635 nm) was amplified, was grown overnight in the 2x TY media at 37°C, diluted and deposited in a concentration of 10^8 cfu/mL for 1 hour. The fluorescence measurements of the sample yielded no signal from the fluorescence bacteria and, having observed the surface with the optical microscope, it was not possible to observe any agglomeration of bacteria in the analyzed zone, suggesting that no interaction between the mannose lines and the pili had taken place. The presence and the operativity of the formers were examined with the deposition of the Concavalin A Alexa Fluor 647 conjugated lectin (1 mg/mL). From the fluorescence measurements obtained using the cya5 laser, it was possible to easily observe the two lines of old and new stock of mannoside, confirming their successful deposition and the lack of non-specific interaction with the other compounds spotted or with the substrate (proving a lack of contamination and good anti-fouling properties with respect to this lectin).
After these results, the growth of the bacteria was modified according to the protocol present in the Experimental section, where antibiotics were added to the cultivation medium in order to stabilize the plasmid and to increase the expression of FimH in the Katushka. Following the deposition of these bacteria on the sample, the fluorescence measurements carried out resulted in the presence of a clear signal coming from the spots of the two mannose lines, although with a strong background from the rest of the surface. However, after a second rinsing with PBS 1X and Milli-Q, the

fluorescence signal was lost and observing the surface with the optical microscope no aggregation of bacteria was visible.

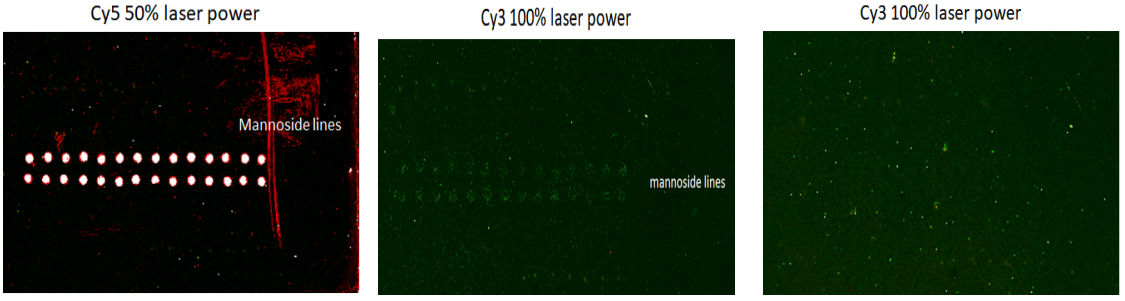

(a) (b) (c)

Figure 8: Fluorescence measurement after ConA (a), Katushka grown with antibiotics (b) deposition and second rinsing (c) on the annealed Au sample, using laser cya3 and cya5 at 50% for (a) and cya3 at 100% of laser power for (b) and (c)

Afterward, the results obtained using this growth of the Katushka *E. Coli* were not entirely reproducible. In fact, despite the fact that the culture and the deposition conditions and the substrate remained the same, the fluorescence signal of the mannose lines measured was found to be weaker or even absent in further experiments (even in case where the deposition time was increased to 2 h).

3.4 *E. Coli* pUT pMM deposition and sandwich sensor

Thus, another strain of the *E. Coli* was used: pUT pMM, a non fluorescence strain of *E. Coli* which was modified to produce FimH positive type 1 piliated bacteria, was grown for 72 hours as described in the experimental section and deposited on the surface in a concentration of 10^8 cfu/mL. After one hour interaction, the surface was examined with the optical microscope, with which it was possible to notice the aggregation of the bacteria on spots aligned along the two mannose lines (one of the spot is shown in Fig 9(a)), although with some minor concentration of physisorbed bacteria on the surface despite the anti-fouling layer.
Having verified the presence of the bacteria on the surface, the sandwich structure (composed by the grafted mannose, the bacteria and the cy5 labelled mannose) described in the introduction was carried out, in order to obtain a strong signal in fluorescence, by the deposition of the fluorescence labelled sugars (mannopyranoside derivates conjugated to Cyanine 5) with a concentration of $5{\cdot}10^{-6}$ M and a rinsing in PBS 1x and Milli-Q. The fluorescence measurement carried out using the 635 nm laser at 100% of its power showed a physisorption of the sugars (and consequent

saturation of the signal) everywhere on the surface. However, when the laser power was reduced to 10% it could be noticed a contrast between the the red background, which could be due to the physisorption, and some saturating points (shown in Fig 9 (c)). Comparing the images obtained with the optical microscope after the mannose deposition (shown in Fig 9 (b)) with the fluorescence measurements, some of the latters could be associated to the bacteria that had been immobilized on the grafted mannose spots, suggesting the presence of a specific interaction with the cyanine5 mannose. Moreover, the observation of the surface with the optical microscope done after the fluorescent mannose deposition showed that the aggregated bacteria were still clearly present in the previous position and, examining the differences between the images obtained with the optical microscope before and after the deposition of the sugars, it was possible to notice that only a small part of the bacteria present on the spots were removed in the latter. This was a concern linked to the idea of the sandwich architecture, since it could have been expected that the bacteria immobilized on the surface by the propargyl mannose would attach to the fluorescence mannose in solution and be desorbed.

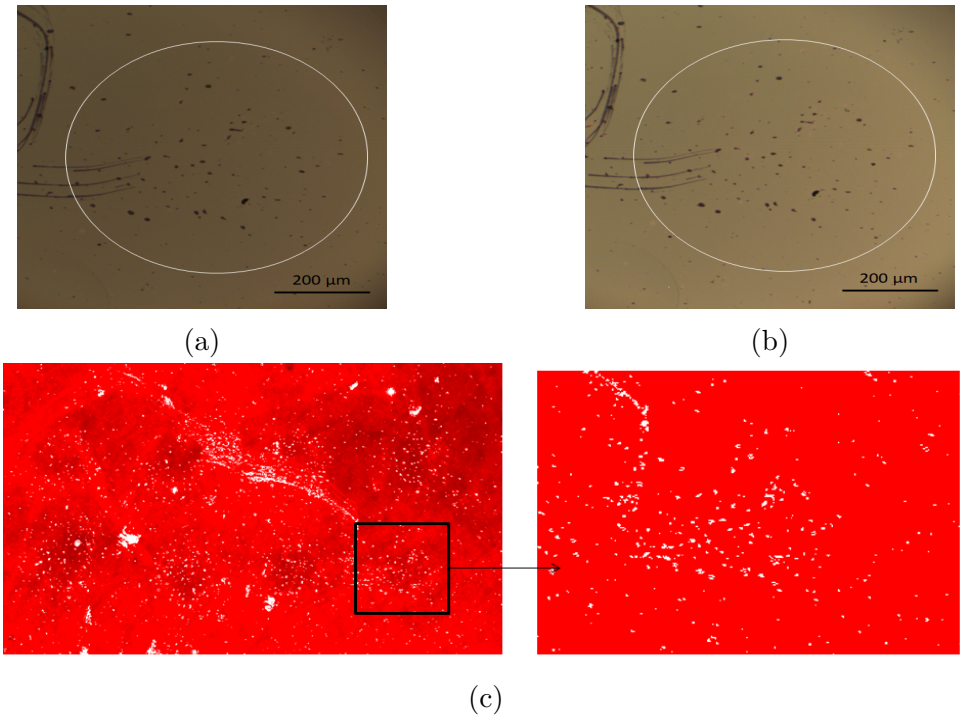

Figure 9: Microscope images (objective x10) of a mannose spot after the deposition of pUT pMM (a) and mannose cya5 (b) and fluorescence measurement (c) of the slide after the deposition of the mannose cya5 using the cya5 laser at 10% of its power

3.5 Analysis of the blocking

As it can be seen in Fig 9 (c), the fluorescence sugars deposited to obtain the readable signal in the sandwich architecture had a clear non-specific physisorption on the surface despite the anti-fouling layer, which lowers the contrast with the signal coming from the detected bacteria. In order to decrease it, on the following samples (the substrate of 4 nm Au not annealed and 3 nm of $aSi_{80\%}C_{20\%}$ and of 4 nm Ag not annealed and 5 nm of $aSi_{95\%}C_{5\%}$) five zones were spotted and different anti-fouling layers of MeO-PEG-alkyne were deposited after the spotting in three of the five zones (the remaining two were left free for further testing). In particular, the concentration of the previously used PEG750 alkyne was increased from 3 mM to 20 mM in the first and second zone, a successive deposition of BSA (Albumin from bovine serum, a commonly used blocking agent for protein or antibody binding whose blocking properties are due to the fact that it binds itself to all the sites which may be available for unspecific binding) 1 mg/mL for 1 hour was performed on the second zone and PEG2000 20 mM was deposited on the third zone. Having prepared the surface, 10^8 cfu/mL of pUT pMM were deposited on the two different samples and using the optical microscope the mannose spots were identified on both of the surfaces. In both cases the concentration of the bacteria on the spots seemed to be lower in the zones blocked with the PEG2000 (as shown in Fig 10 and 11) but no particular observation could be done regarding the non-specific absorption of the bacteria. Moreover, the spots resulting from the agglomeration of the bacteria on the Ag sample seemed to be bigger and more dense than the ones obtained in the Au sample. The latter could be due to the lower concentration of the C in the amorphous layer of the substrates, which increases the concentration of Si-H bonds that can be grafted by the surface functionalization. Furthermore, in both of the samples (prepared simultaneously) it could be observe an interaction between the pUT pMM and the lactose lines, which suggest a possible contamination of the spots (Fig 12).

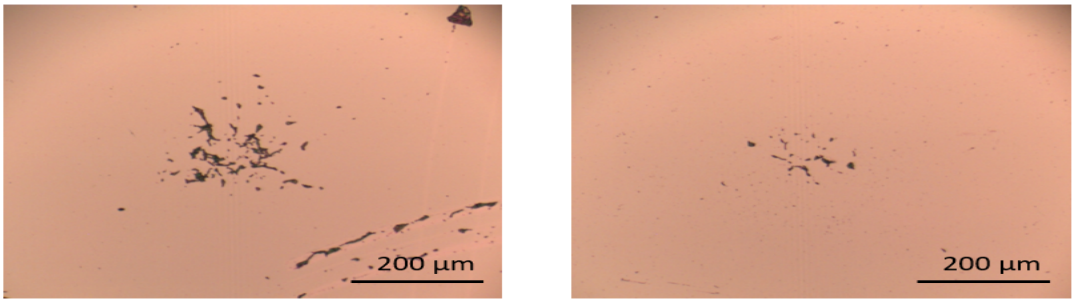

(a) (b)

Figure 10: Microscope images (objective x10) of a mannose spot after the deposition of pUT pMM on the zone blocked with PEG750 20 mM + BSA (a) and PEG2000 20 mM (b) of the not annealed Au slide

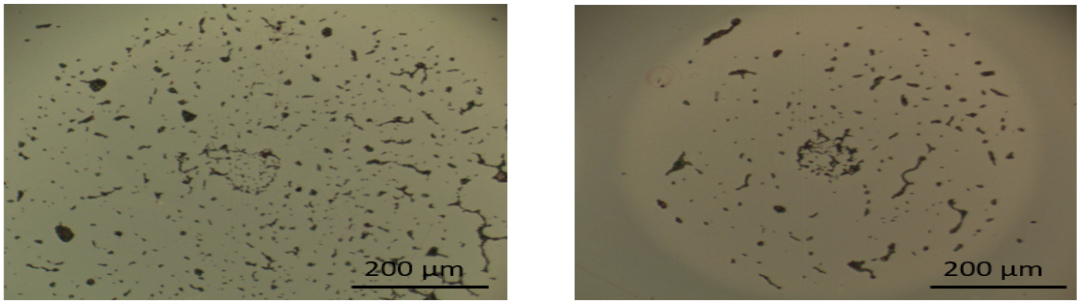

(a) (b)

Figure 11: Microscope images (objective x10) of a mannose spot after the deposition of pUT pMM on the zone blocked with PEG750 20 mM (a) and PEG2000 20 mM (b) of the not annealed Ag slide

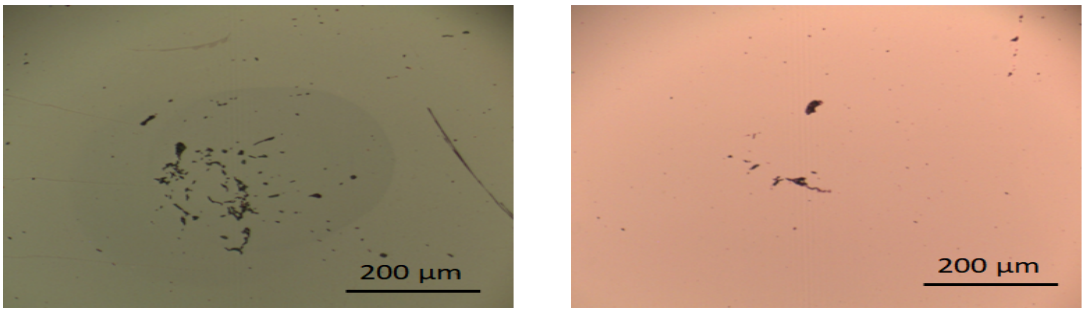

(a) (b)

Figure 12: Microscope images (objective x10) of a lactose spot after the deposition of pUT pMM on the not annealed Ag slide (a) and the not annealed Au slide (b)

Subsequently, a lower concentration ($5{\cdot}10^{-7}$ M) of fluorescent mannose was used. Taking the fluorescence measurements with the 635 nm laser at 100% of its power, all the zones saturate completely (the sugars are completely physisorbed despite the changes done). However, decreasing the power to 10% the presence of saturating points on the mannose (and lactose) lines were visible over the background (as shown in Fig 13). Moreover, taking an average measure of the background intensity along a y cut in the different zones, the Ag substrate resulted to be the one with the highest noise signal and, in general, the zone blocked with the PEG2000 had a slight higher value. No particular difference of the noise signal was found due to the addition of the BSA.

Observing the samples with the optical microscope, a clear correlation between the saturating points detectable on top of the background noise in the fluorescence measurements and the bacteria present on the spots was visible, suggesting an interaction between the latter and the labelled element deposited.

However, a noticeable loss of the bacteria after the deposition of the cyanine 5 mannose was observed in the Ag sample, which could be due to either the rinsing steps

or to the presence of a higher concentration of mannose deposited in solutions with respect to the ones grafted on the spots (to have a quantitative value of the concentration of the sugars on the spots a further analysis is required). This also could suggest that part of the bacteria observed on the mannose spots in the silver sample could be just physisorbed on the surface.

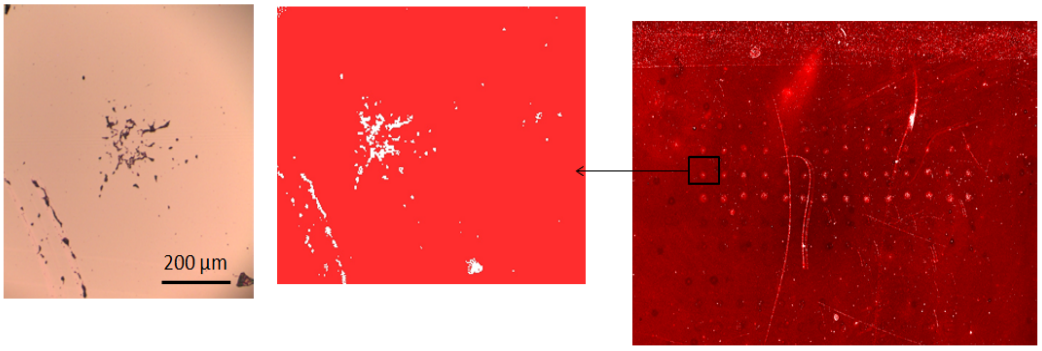

Figure 13: Comparison between the fluorescence signal obtained with 10% of the cy5 laser (right side) and the bacteria visible using the optical microscope (left side) in the zone blocked with PEG750 and BSA on the not annealed Au substrate

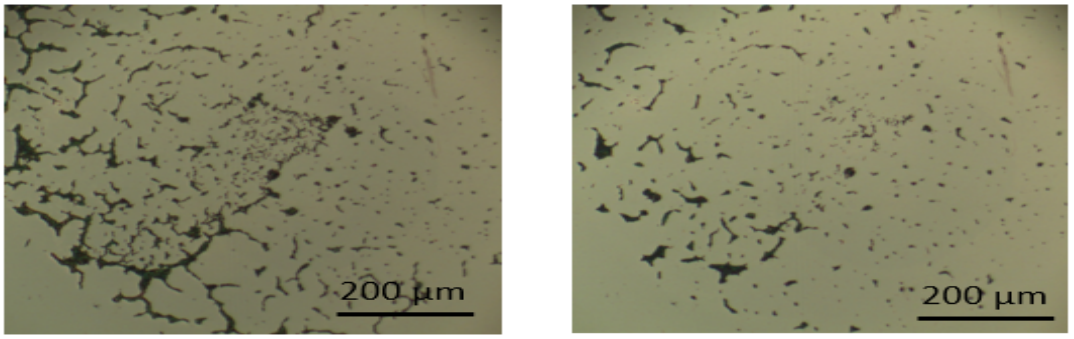

(a) (b)

Figure 14: Microscope images (objective x10) of a mannose spot after the deposition of put pmm (a) and mannose (b) on the zone blocked with PEG750 20 mM of the not annealed Ag slide

In general, using this parameters the fluorescent sugars were still physisorbed everywhere on the surface generating a high background signal that limited the contrast with the signal that indicates the detection of the bacteria. Thus, in order to decrease the noise signal coming from the background, the physisorption of the mannose directly on the surface was examined. This was done by depositing, after a further dilution to a concentration of $5{\cdot}10^{-9}$ M, the labelled sugars onto an old sample (3 nm annealed Au) were three different blocking (PEG750, PEG2000 and PEG5000

3 mM) agents were grafted, to examine whether a longer hydrophilic chain would increase the anti-fouling properties, and adding a supplementary rinsing step in PBS SDS 0.1% for 5 minutes afterwards. The first fluorescence measurement was carried out after a 15 minutes deposition of the mannose and a rinsing in PBS Tween 0,005% (5 min) and Milli-Q (2 min). While the sugars were still physisorbed on the entire surface in all the zones examined, the noise signal after the dilution was lower with respect to the one obtained in the sandwich and it did not present saturation using the 635 nm laser at 100% of its power. Moreover, the background present in the zone blocked with PEG750 had a lower intensity with respect to the other ones (taking the average value of the intensity along a y cut of the different zones, the one with PEG750 had a value of $\sim$ 11500, the one with PEG2000 had a value of $\sim$ 17200 while the one with PEG5000 had a value of $\sim$ 18800). Moreover, after a thorough second rinse in PBS SDS 0.1%, the fluorescence background obtained using the cya5 laser at 100% of the power resulted drastically decreased in all of the zones (the average intensity along the y cut in this case was of $\sim$ 4600 for the zone blocked with PEG750, of $\sim$ 6900 for the zone with PEG2000 and of $\sim$ 5700 for the zone with PEG5000). These results seemed to suggest that an increase of the hydrophilic length of the poly(ethylene glycol) did not improve the anti-fouling of the surface with respect to the surface and that a stronger cleaning step may be required in order to reduce the presence of physisorbed mannose.

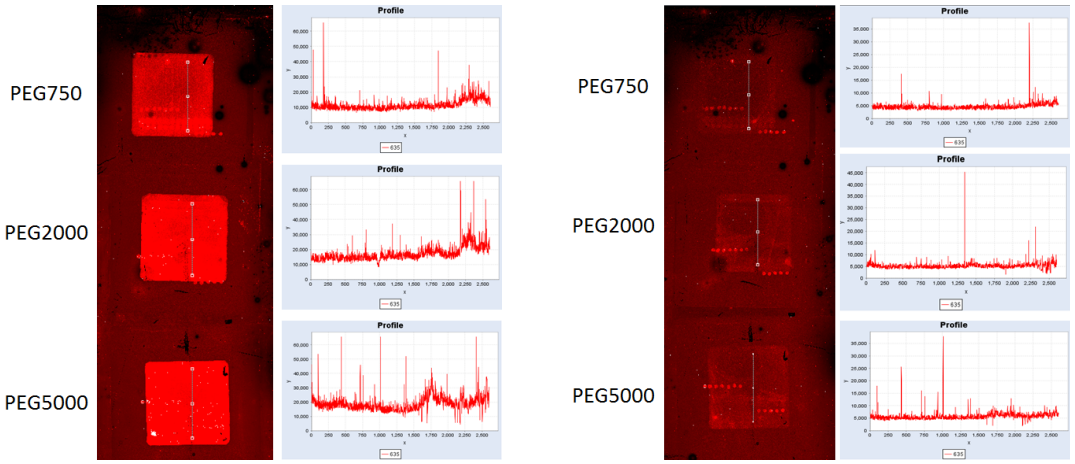

(a) (b)

Figure 15: Fluorescence measurement of the deposited cyanine 5 conjugated mannose after the rinsing with PBS Tween 0.005% (a) and PBS SDS 0.1% in the different zones of the Au sample (from top to bottom the blocking agent used is PEG750 3 mM, PEG2000 3 mM and PEG5000 3mM)

Having observe that an increase in the length of the chain of the PEG did not decrease the non-specific adsorption of the sugars, the last zones of the Ag sample used in the section 3.4 were blocked using 20 mM of PEG750. After the deposition

of 10^8 cfu/mL of pUT pMM (which were left in the stationary oven at 37°C for 72 hours instead of 48 hours) onto the surface, the sample was observed with the optical microscope, where it was possible to see the aggregation of the bacteria along four lines (along the mannose, where the shape of the spots were difficult to make out because the mannose drops spotted were so big that they intersected one another, and the lactose lines, where the agglomerated bacteria were less concentrated). In general the concentration of the bacteria seemed to be lower than the one obtained previously on the zone of the Ag sample blocked with PEG750 20 mM (Fig. 11), which may be due to the growth conditions.

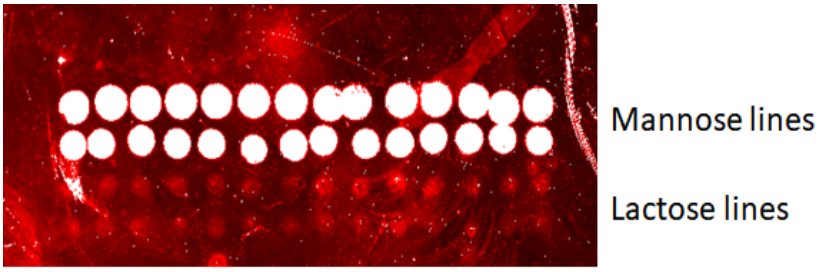

Figure 16: Fluorescence measurement of the deposited ConA on the Ag sample

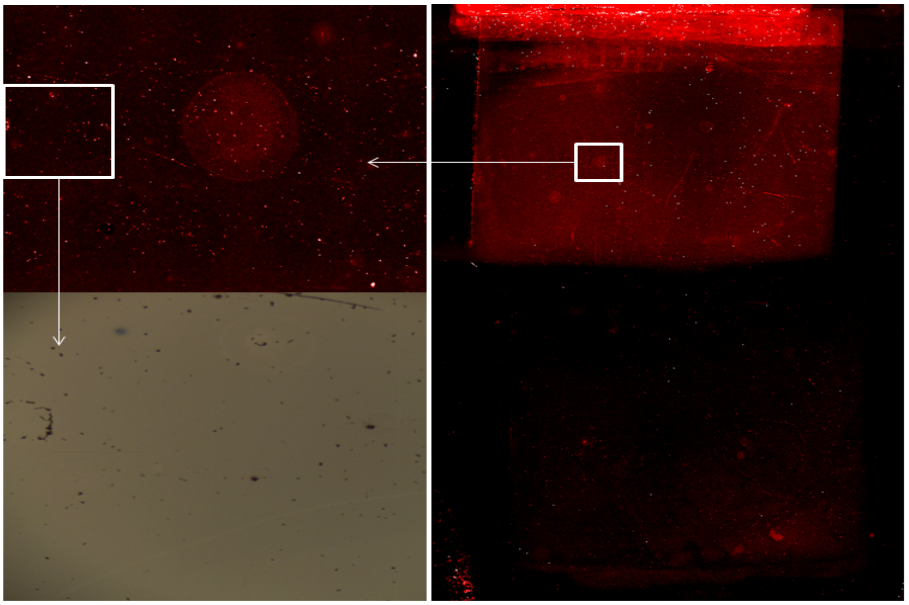

Figure 17: Fluorescence measurement of the deposited cyanine 5 conjugated mannose $5{\cdot}10^{-9}$ M (right image, top zone) and $5{\cdot}10^{-10}$ M (right image, bottom zone) on the Ag sample, left image top is the zoom on the mannose line and on the bottom the correlated image of the bacteria obtained with the optical microscope

The presence of contamination of the lactose spots was verified by the deposition of

ConA (fluorescent protein that interacts specifically with the mannose) on a different zone. In fact, as it is shown in Fig 16, while a strong signal was visible coming from the two mannose lines, a weaker signal was also visible coming from the lactose lines. Following this, the fluorescent mannose were deposited for 15 minutes on the zone where we had deposited the pUT pMM, using a different concentration ($5{\cdot}10^{-9}$ M and $5{\cdot}10^{-10}$ M) in the two zones. The fluorescence measurement carried out showed no signal coming from the latter zone whereas on the former it was possible to notice the presence of saturating points on the red background. While it was possible to correlate some of these points to the images obtained from the optical microscope, the contrast obtained was very weak and it was difficult to distinguish the signal coming from the background and the one coming from the detection of the bacteria (as shown in Fig 17).

3.6 Sandwich architecture without MEF

For the last attempt made to decrease the background signal of the physisorbed cy5 mannose, the sandwich architecture was repeated, using a slightly different surface functionalization for the grafting of the mannose (as described in the experimental section), using a substrate composed by a clean glass slide on top of which 3 nm of aSi:H were deposited by PECVD at 250°C, removing the effect of the metallic layer on the final signal. In this case the bacteria deposited in a concentration of 10^8 cfu/mL were the Katushka strain, using the first growth conditions without adding the antibiotics. Having observed that in this experiment an agglomeration of bacteria was present on the spots, the cy5 mannose were deposited on the zone with a concentration of $5{\cdot}10^{-9}$ M. From the fluorescence measurements (Fig 18), it was possible to observe that, while the background noise had a lower intensity with respect to the one found at the same conditions in the Ag sample (Fig 17), the signal coming from the mannose spots, while not saturating, was clear enough to form a higher contrast than the one obtained in the previous experiment. This seems to suggest that, while the metallic layer provides an enhancement for the fluorescence of the mannose physisorbed on the surface, the ones interacting specifically with the immobilized bacteria may not benefit from the same enhancement, possibly due to the fact that in the second case the fluorophore is too distant from the nanostructured metallic layer. This was also noticed comparing the fluorescence intensity signal obtained simply by the Katushka bacteria deposited on the sample with a 4 nm layer of annealed Au (Fig 8 (b)) and the one obtained from the sample without the metallic layer (Fig 19), which resulted similar.
However, comparing the images obtained with the optical microscope before and after the deposition of the bacteria, a significant loss of the bacteria on the spots

can be noticed (Fig 18), which, as in the case of the Ag slide, could be due to either the rinsing step or a higher concentration of the mannose in solution with respect to the grafted ones and could signify that the bacteria observed on the spots could be just physisorbed.

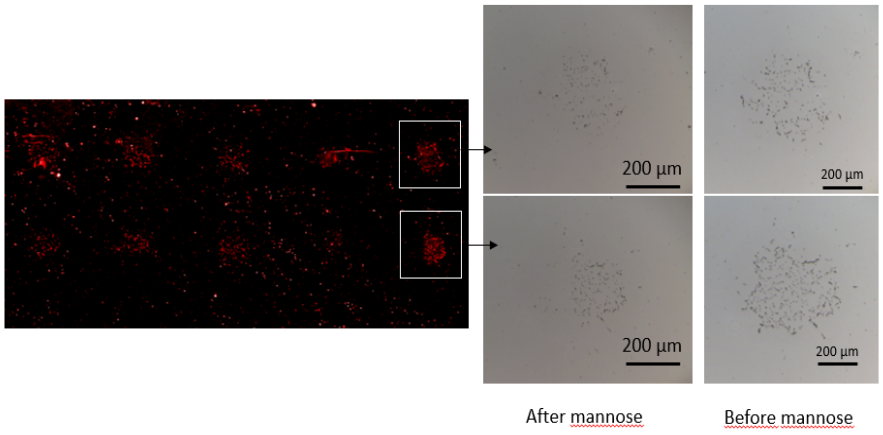

Figure 18: Fluorescence measurement of the deposited cyanine 5 conjugated mannose $5{\cdot}10^{-9}$ M (left image) on the aSi sample and correlated images of the bacteria obtained with the optical microscope (right, before and after the deposition of the fluorescent mannose)

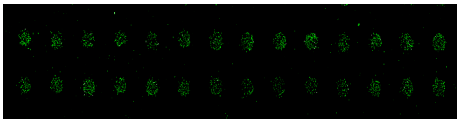

Figure 19: Fluorescence measurement of the deposited Katushka bacteria on the aSi sample using the cy3 laser at 100%

4 Conclusions

During the course of this internship, an optical biosensor for the detection of the *E. Coli* was implemented. In particular, a sandwich strategy composed of mannose grafted on the surface to immobilize the bacteria, the bacteria itself and a second cyanine5 labelled mannose was used to obtain a fluorescence signal enhanced by the presence of a metallic nano-structured layer. The plasmon resonance of three different metallic materials was studied and optimized for the working wavelengths by a deposition of an amorphous silicon-carbon alloy by PECVD. On these surfaces, the biosensor was implemented by a robust and reproducible grafting of the different glycans through several functionalization steps. Two strains of *E. Coli* were tested, the first of which (Katushka), despite an optimization of the growth conditions, did not give reproducible results. The sandwich architecture was implemented on

the second strain (pUT pMM) showing the presence of saturating spots that could be associated with the bacteria observed with the optical microscope. However a non-specific physisorption of the fluorescence mannose was observed on the surface. With an optimization of the anti-fouling layer and of the concentration of the sugars, this background noise was reduced but the contrast with the signal coming from the bacteria detected was weak. A final test using a sample without the presence of the metallic layer seemed to suggest an enhancement of the signal from the physisorbed mannose and a lack of enhancement on the signal coming from the interaction with the bacteria.
While the contrast observed in the fluorescence images seems to suggest the formation of the sandwich interaction, further experiments to verify these results and the various hypothesis are needed. Moreover, further optimizations of the sensor (among which a possible modification in the architecture to be able to exploit the MEF effect) are needed to be able to decrease the LOD (in all the experiments done the value of the concentration of the bacteria of 10^8 cfu/mL, too high for an efficient sensor). Furthermore, the grafting of sugars for the immobilization of the bacteria and the presence of the metallic layer could studied to be used to implement a sensor based on the SERS effect, which allows the identification of the bacteria detected thanks to the characteristic peaks obtained, as it is currently studied by the PhD student Cassiana Andrei.

References

[1] Mohanty, Saraju, 2002, Biosensors: A Survey Report.
[2] Jie Yang, Study of the multivalent carbohydrate/protein interactions on silicon biosensors, Chemical Science, Ecole polytechnique X, 2014
[3] Touahir, L. PhD thesis (PMC, Ecole Polytechnique), 2010
[4] Kline, K.A., Falker, S., Dahlberg, S., Normark, S., Henriques-Normark, B., 2009. Bacterial adhesins in host-microbe interactions. Cell Host Microbe 5, 580–592.
[5] Joel D. Schilling, Matthew A. Mulvey, Scott J. Hultgren, Structure and Function of Escherichia coli Type 1 Pili: New Insight into the Pathogenesis of Urinary Tract Infections, The Journal of Infectious Diseases, Volume 183, Issue Supplement_1, 1 March 2001, S36–S40
[6] Lakowicz, Joseph. (2006). Principles of Fluorescence Spectroscopy.
[7] Eric C. Le Ru, Pablo G. Etchegoin, Principles of Surface-Enhanced Raman Spectroscopy, Elsevier, 2009.
[8] A. Datsenko, Kirill Wanner, Barry. (2000). Datsenko KA, Wanner BL., One-step inactivation of chromosomal genes in Escherichia coli K-12 using PCR products, Proc Natl Acad Sci USA 97: 6640-6645, Proceedings of the National Academy of Sciences of the United States of America, 97, 6640-5.
[9] Minion FC, Abraham SN, Beachey EH, Goguen JD. The genetic determinant of adhesive function in type 1 fimbriae of Escherichia coli is distinct from the gene encoding the fimbrial subunit. Journal of bacteriology. 1986;165(3):1033–6.
[10] Florent, Colas Barchiesi, Dominique Kessentini, Sameh Toury, Timothée Lamy de la Chapelle, M, (2015), Comparison of adhesion layers of gold on silicate glasses for SERS detection, Journal of Optics, 17, 114010.
[11] Aouani, Heykel Wenger, Jerome Gérard, Davy Rigneault, Hervé Devaux, Eloïse W Ebbesen, Thomas Mahdavi, Farhad Xu, Tingjun Blair, Steve, (2009). Crucial Role of the Adhesion Layer on the Plasmonic Fluorescence Enhancement, ACS nano, 3, 2043-8.
[12] Habteyes, Terefe Dhuey, Scott Wood, Erin Gargas, Daniel Cabrini, Stefano James Schuck, P Paul Alivisatos, A Leone, Stephen, (2012), Metallic Adhesion Layer Induced Plasmon Damping and Molecular Linker as a Nondamping Alternative, ACS nano, 6, 5702-9.
[13] Francolini, Iolanda Vuotto, Claudia Piozzi, Antonella Donelli, Gianfranco, (2017), Antifouling and antimicrobial biomaterials: an overview, APMIS, 125, 392-417.